On the Theory and Errata to "Data Transfer From RZ-OOK to RZ-BPSK by Polarization-Insensitive XPM in a Passive Birefringent Nonlinear AlGaAs Waveguide"

W. Astar, Brice M. Cannon, Tanvir Mahmood, Paveen Apiratikul, G. A. Porkolab, C. J. K. Richardson, and Gary M. Carter, *Life Fellow, IEEE, Fellow, OSA*

***Abstract*—The dependence of the nonlinear coefficients on the transverse profiles of the pump and the probe fields, which is especially important for a highly anisotropic device such as the $Al_{0.18}Ga_{0.82}As$ waveguide, was not explicitly stated in our paper "Data transfer from RZ-OOK to RZ-BPSK by polarization-insensitive XPM in a passive birefringent nonlinear AlGaAs waveguide." The four-wave mixing efficiency was also incorrectly presented to depend on the square of the device physical length. Lastly, the influence of the fiber-waveguide coupling coefficient was neglected with insufficient justification, leading to an inaccurate general expression for the detected voltage.**

***Index Terms*—Birefringence, cross-phase modulation, integrated optics, nonlinear optical signal processing, nonlinear waveguides.**

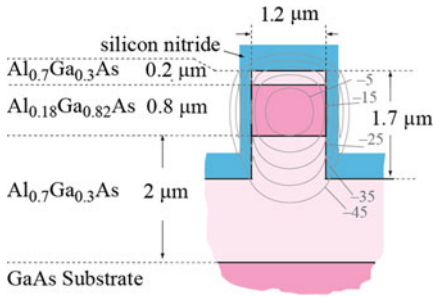

Fig. 1. Cross-section of the $Al_{0.18}Ga_{0.82}As$ waveguide, and calculated optical mode profile, showing power dB-contours. Fig. 1(a) in [9] erroneously showed the waveguide ridge width as "0.6–2.5 μm." At the pump wavelength (1559 nm), the refractive index of the 0.8-μm-thick guiding layer is 3.27, while that (n_{clad}) of the cladding is 3.02 [8].

I. Introduction

THE propagation of either the pump $(\mu = 1)$ or the probe $(\mu = 2)$ field envelopes A in the z-direction, in a nonlinear, birefringent waveguide can be described by a pair of coupled nonlinear Schrodinger equations (NLSE) [1], [2], as shown in (1). The implied dependence of an envelope in (1) is (z, t), which has been suppressed for compactness. The co-ordinate axes are assumed to be coincident with the birefringence axes of the waveguide, since the birefringence axes are fixed over the entire length of the device [3]. The x- and y-coordinates are, respectively, taken to be parallel and perpendicular to the substrate of the waveguide. The x-component of the NLSE (1) corresponds to the quasi-TE (QTE) mode, while the y-component, to the quasi-TM (QTM) mode. Since the $Al_{0.18}Ga_{0.82}As$ waveguide (see Fig. 1) refractive index contrast $\Delta n/n_{\mathrm{clad}} \approx 0.08$, both the QTE and the QTM modes will be hybrid, each with six spatial field profiles in total, three components in each of the electric and the magnetic fields. The eigenvalues of the QTE and QTM modes are respectively given by β_x and β_y and along with the spatial profiles of the modes, are all found at a specific frequency ω_μ by the full-vector finite-difference method (FV-FDM) [4]. Based on FV-FDM simulations for the waveguide, it was found that the x-component was dominant for the QTE-mode, whereas the y- component was dominant for QTM-mode, both shown in Fig. 2. The constant coefficient E in (1) as shown at the bottom of the next page, is known to be 1/3 for a linearly birefringent fiber [2]. For a birefringent $Al_{0.18}Ga_{0.82}As$ waveguide at half-the-bandgap grown on a [0 0 1]-oriented GaAs substrate, the constant E was found to be approximately 1/2 [5], [6]. It was also found that the Kerr-index was different for the two polarizations in the neighborhood of 1550 nm, by at least 5% [6], [7]. In general, the nonlinear coefficients (γ) for SPM and XPM can be estimated from the $Al_{0.18}Ga_{0.82}As$ Kerr-index data [6], linear index data [8] for the FV-FDM [4], and using the theory from [2]:

Manuscript received August 7, 2013; revised September 18, 2013; accepted October 16, 2013. Date of publication October 27, 2013; date of current version November 18, 2013.

W. Astar is with the Laboratory for Physical Sciences (LPS), College Park, MD 20740 USA and also with the Center for Advanced Studies in Photonic Research (CASPR), Baltimore, MD 21250 USA (e-mail: notilos@lps.umd.edu).

P. Apiratikul, G. A. Porkolab, and C. J. K. Richardson are with LPS, Park, MD 20740 USA (e-mail: paveen@lps.umd.edu; porkolab@lps.umd.edu; richardson@lps.umd.edu).

B. M. Cannon, T. Mahmood, and G. M. Carter are with LPS, College Park, MD 20740 USA, and with CASPR, Baltimore, MD 21250 USA, and also with the Department of Computer Science and Electrical Engineering, University of Maryland Baltimore County (UMBC), Baltimore, MD 21250 USA (e-mail: cannonb1@lps.umd.edu; tanvir1@lps.umd.edu; carter@lps.umd.edu).

Color versions of one or more of the figures in this paper are available online at http://ieeexplore.ieee.org.

Digital Object Identifier 10.1109/JLT.2013.2287491

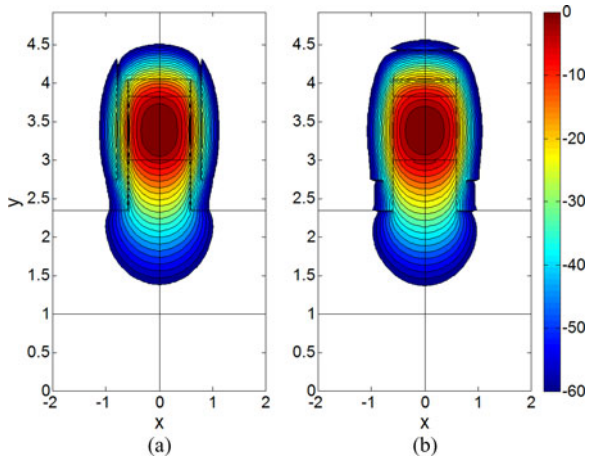

Fig. 2. Some of the transverse field components of the QTE- and QTM-modes for the pump (1559 nm) obtained using linear index data [8] along with FV-FDM [4], and superimposed on the cross-section of the waveguide (Fig. 1): (a) M_{xx} in equation (2), (b) M_{yy} in equation (2). These are the respective dominant components of the QTE- and QTM-modes, based on simulations. The spatial field components of the probe (1547 nm) are similar, since the wavelengths of the pump and the probe differed by $<1\%$. All dimensions are in μm.

$$\gamma_{\mu\zeta\sigma\eta} = \frac{\omega_\mu n_{2\sigma}(\omega_\mu)}{c} \times \frac{\iint |M_{\sigma\sigma}(x,y,\omega_\mu)|^2 \, |M_{\eta\eta}(x,y,\omega_\zeta)|^2 \, dS}{\left(\iint |M_{\sigma\sigma}(x,y,\omega_\mu)|^2 \, dS\right)\left(\iint |M_{\eta\eta}(x,y,\omega_\zeta)|^2 \, dS\right)} = \frac{\omega_\mu n_{2\sigma}(\omega_\mu)}{cA_{\mathrm{eff}\,\sigma}(\omega_\mu)} \, \delta_{\zeta\mu} \, \delta_{\eta\sigma}; \quad \zeta \in \{\mu,\ \nu\}; \quad \sigma,\eta \in \{x,y\}; \quad \mu,\nu \in \{1,\ 2\} \tag{2}$$

and the kernel reduces to $1/A_{\mathrm{eff}\,\sigma}$ (where $A_{\mathrm{eff}\,\sigma}$ is the effective area for the σ-polarization mode) only when $\eta = \sigma$ for SPM $(\zeta = \mu)$, otherwise it is termed the shape factor. In (2), c is the speed of light in vacuum. $M_{\sigma\sigma}(x, y, \omega_\mu)$ is the dominant component of the electric field of the σ-polarization mode, at the μ-th frequency ω_μ. dS is the differential transverse area element, and the region of integration is the cross-section of the waveguide. The Kerr-index $(n_{2\sigma})$ is shown to be dependent on whether the mode is QTE $(\sigma = x)$ or QTM $(\sigma = y)$, and this dependence is reflected in the subscript σ. The influence of the spatial profiles, and the polarization-dependence of the Kerr-index $(n_{2\sigma})$ on the nonlinear coefficient (2) was erroneously neglected in our original paper [9]. In general, the nonlinear coefficient (2) depends on whether the nonlinearity is due to co-polarized $(\eta = \sigma)$ or cross-polarized $(\eta \neq \sigma)$ SPM $(\zeta = \mu)$; or due to co-polarized $(\eta = \sigma)$, or cross-polarized $(\eta \neq \sigma)$ XPM $(\zeta \neq \mu)$. The various XPM coefficients for the probe are found in Table I, and are more accurate than those in [9, Table I], since they account for the polarization dependence of the Kerr index. The last three terms in each axial equation in (1) are interpreted to represent birefringence-dependent, degenerate and partially degenerate FWM, and not XPM. The XPM and FWM terms in the NLSE both have a cubic dependence on the pump and the probe fields. The distinction between XPM and FWM is based on the convention that the field components are automatically phase-matched for XPM, which is not the case for FWM [2]. The first term thus expresses fully degenerate, *intra*-channel FWM. The other two terms represent partially degenerate, *inter*-channel FWM. The constants F can also be device-dependent, just as the XPM constants E as previously noted, is different for fibers and semiconductor waveguides. The FWM terms will also have shape factors [10], described in general in (3) as shown at the bottom of the next page, which were also overlooked in our original paper [9]. It was found in [9] that the contribution due to FWM may be significantly mitigated by choosing [2], [11]

$$L\Delta\beta > K\pi \quad \text{or} \quad L > KL_c \quad |\, K \gg 1\,. \tag{4}$$

In the original paper [9], we discussed the elimination of the FWM terms in (1), by considering FWM efficiency (a non-dimensional quantity) for a general FWM phase term $\exp(\pm iz\Delta\beta)$, with its dependence on the phase-mismatch $\Delta\beta$

TABLE I
NONLINEAR (XPM) COEFFICIENTS FOR THE PROBE (THE KERR-INDICES WERE OBTAINED FROM [6])

QTE (x)		QTM (y)	
γ_{21xx}	γ_{21xy}	γ_{21yy}	γ_{21yx}
0.88	0.84	0.76	0.79

$$\begin{aligned}
&\frac{\partial A_{\mu\,x}}{\partial z} + \beta_{1\mu\,x}\frac{\partial A_{\mu\,x}}{\partial t} + \frac{i\beta_{2\mu x}}{2}\frac{\partial A^2_{\mu\,x}}{\partial t^2} - \frac{\beta_{3\mu x}}{6}\frac{\partial A^3_{\mu\,x}}{\partial t^3} = -\frac{\alpha_{\mu\,x}}{2}A_{\mu\,x} + \left(i\gamma_{\mu\mu xx}\,|A_{\mu\,x}|^2 + 2iE\gamma_{\mu\mu xy}\,|A_{\mu\,y}|^2\right)A_{\mu\,x} \\
&\quad + 2\left(i\gamma_{\mu\nu xx}\,|A_{\nu\,x}|^2 + iE\gamma_{\mu\nu xy}\,|A_{\nu\,y}|^2\right)A_{\mu\,x} + iF_{1x}\kappa_{\mu yyx}A^2_{\mu\,y}A^*_{\mu\,x}\exp(2iz\Delta\beta_\mu) + iF_{2x}\kappa_{\nu yyx}A_{\mu\,y}A_{\nu\,y}A^*_{\nu\,x} \\
&\quad \times \exp[iz\ (\Delta\beta_1 + \Delta\beta_2)] + iF_{2x}\kappa_{\nu yxy}A_{\mu\,y}A_{\nu\,x}A^*_{\nu\,y}\exp[iz\ (\Delta\beta_1 - \Delta\beta_2)] \\
&\frac{\partial A_{\mu\,y}}{\partial z} + \beta_{1\mu\,y}\frac{\partial A_{\mu\,y}}{\partial t} + \frac{i\beta_{2\mu y}}{2}\frac{\partial A^2_{\mu\,y}}{\partial t^2} - \frac{\beta_{3\mu y}}{6}\frac{\partial A^3_{\mu\,y}}{\partial t^3} = -\frac{\alpha_{\mu\,y}}{2}A_{\mu\,y} + \left(i\gamma_{\mu\mu yy}\,|A_{\mu\,y}|^2 + 2iE\gamma_{\mu\mu yx}\,|A_{\mu\,x}|^2\right)A_{\mu\,y} \\
&\quad + 2\left(i\gamma_{\mu\nu yy}\,|A_{\nu\,y}|^2 + iE\gamma_{\mu\nu yx}\,|A_{\nu\,x}|^2\right)A_{\mu\,y} + iF_{1y}\kappa_{\mu xxy}A^2_{\mu\,x}A^*_{\mu\,y}\exp(-2iz\Delta\beta_\mu) + iF_{2y}\kappa_{\nu xxy}A_{\mu\,x}A_{\nu\,x}A^*_{\nu\,y} \\
&\quad \times \exp[-iz\ (\Delta\beta_1 + \Delta\beta_2)] + iF_{2y}\kappa_{\nu xyx}A_{\mu\,x}A_{\nu\,y}A^*_{\nu\,x}\exp[-iz\ (\Delta\beta_1 - \Delta\beta_2)] \\
&\nu = 3 - \mu\ ; \quad \nu,\ \mu \in \{1,\ 2\}
\end{aligned} \tag{1}$$

[11] and in the absence of propagation loss, stated here as

$$\text{sinc}^2\left(L\Delta\beta/2\right) \tag{5}$$

while [9] incorrectly included a multiplicative factor of L^2, where L is the physical length of the waveguide. It was also found that the efficiency vanishes whenever the following *discrete* condition is met:

$$L\Delta\beta = 2m\pi \quad \text{or} \quad L = 2mL_c \quad \left| m \in \mathbb{Z}^+ \right. . \tag{6}$$

The minimum requirement occurs for $m = 1$. Although the discrete condition can guarantee a local minimum, complete extinction of the efficiency (5) is not possible when the propagation loss is significant [9], which was the case for the waveguide, and which was indeed reflected in our experimental results (see Fig. 4 in [9]). Upon elimination of the FWM *F*-terms, the NLSE (1) may then be solved in the non-dispersive XPM regime for a birefringent device as before (see eq. (17) in [9]), with the following solutions in the reference frame of the QTE-mode, as (7) shown at the bottom of the page, where the nonlinear coefficients (γ) are more accurately given by (2). Having solved for the field envelopes $A_\sigma(L,T)$, the QTE-mode $(\sigma = x)$ and QTM-mode $(\sigma = y)$ can each be subsequently described by the electromagnetic (EM-) field $(\mathbf{E}_\sigma, \mathbf{H}_\sigma)$ at the output of the device

$$\begin{cases} \mathbf{E}_\sigma(\mathbf{r},\omega,T) = \sum_{\xi=x}^{z} \xi\, A_\sigma(L,T) M_{\sigma\xi}(\mathbf{r},\omega)\, e^{i\omega T - i\beta_\sigma(\omega)L} \\ \qquad\qquad = A_\sigma(L,T)\mathbf{E}_\sigma(\mathbf{r},\omega) \\ \mathbf{H}_\sigma(\mathbf{r},\omega,T) = \sum_{\xi=x}^{z} \xi\, A_\sigma(L,T) N_{\sigma\xi}(\mathbf{r},\omega)\, e^{i\omega T - i\beta_\sigma(\omega)L} \\ \qquad\qquad = A_\sigma(L,T)\mathbf{H}_\sigma(\mathbf{r},\omega) \end{cases} . \tag{8}$$

The subscript μ which was associated with the signal frequency in (7), was suppressed in (8) to simplify the notation. The frequency (ω) dependence reflects the presence of two signals (the pump and the probe) in the waveguide. While the field components M and N, as well as the eigenvalues β_σ are all first found by FV-FDM [4], the field envelopes A_σ are then subsequently found from the vector non-linear Schrodinger equation (NLSE) as explained previously. The dependence of the profiles and the eigenvalues on the signal frequency is due to material and waveguide dispersion. For a z-invariant waveguide, the spatial dependence of the field components M and N is reduced to that on the transverse coordinates, r_T or (x, y) [12].

II. Detection of the DBPSK Signal

In the original paper [9], the RZ-BPSK probe is detected as a DBPSK signal. The DBPSK receiver consists of an asymmetric Mach–Zehnder interferometer (AMZI), whose two outputs are

$$\kappa_{\zeta\eta\varepsilon\rho} = \frac{\omega_\mu n_{2\sigma}(\omega_\mu)}{c} \frac{\iint M^*_{\sigma\sigma}(x,y,\omega_\mu) M_{\eta\eta}(x,y,\omega_\mu) M_{\varepsilon\varepsilon}(x,y,\omega_\zeta) M^*_{\rho\rho}(x,y,\omega_\zeta) dS}{\left(\iint |M_{\sigma\sigma}(x,y,\omega_\mu)|^2 dS \iint |M_{\eta\eta}(x,y,\omega_\mu)|^2 dS \iint |M_{\varepsilon\varepsilon}(x,y,\omega_\zeta)|^2 dS \iint |M_{\rho\rho}(x,y,\omega_\zeta)|^2 dS\right)^{1/2}};$$
$$\sigma,\, \eta,\, \varepsilon,\, \rho \in \{x,y\}, \quad \zeta \in \{\mu,\nu\} \tag{3}$$

$$\begin{aligned} A_{\mu x}(L,T) &= A_{\mu x}(0,T) \\ &\cdot e^{i\phi_{\mu x}} e^{-\alpha_{\mu x}L/2} \exp\left[\begin{array}{l} i\gamma_{\mu\mu xx} P_{\mu x}(0,T) L_{\mu \mathrm{eff}\, x} + 2iE\gamma_{\mu\mu xy} \int_0^L P_{\mu y}\left(0,\, T + \xi\frac{\Delta\tau}{L}\right) e^{-\alpha_{\mu y}\xi} d\xi \\ +2i\gamma_{\mu\nu xx} \int_0^L P_{\nu x}\left(0,\, T + \xi\frac{\Delta T_1}{L_W}\right) e^{-\alpha_{\nu x}\xi} d\xi \\ +2iE\gamma_{\mu\nu xy} \int_0^L P_{\nu y}\left(0,\, T + \xi\left(\frac{\Delta T_1}{L_W} + \frac{\Delta\tau}{L}\right)\right) e^{-\alpha_{\nu y}\xi} d\xi \end{array} \right] \\ A_{\mu y}(L,T) &= A_{\mu y}(0, T+\Delta\tau) \\ &\cdot e^{i\phi_{\mu y}} e^{-\alpha_{\mu y}L/2} \exp\left[\begin{array}{l} i\gamma_{\mu\mu yy} P_{\mu y}(0,T+\Delta\tau) L_{\mu \mathrm{eff}\, y} + 2iE\gamma_{\mu\mu yx} \int_0^L P_{\mu x}\left(0,\, T+\Delta\tau - \xi\frac{\Delta\tau}{L}\right) e^{-\alpha_{\mu x}\xi} d\xi \\ +2i\gamma_{\mu\nu yy} \int_0^L P_{\nu y}\left(0,\, T+\Delta\tau + \xi\frac{\Delta T_1}{L_W}\right) e^{-\alpha_{\nu y}\xi} d\xi \\ +2iE\gamma_{\mu\nu yx} \int_0^L P_{\nu x}\left(0,\, T+\Delta\tau + \xi\left(\frac{\Delta T_1}{L_W} - \frac{\Delta\tau}{L}\right)\right) e^{-\alpha_{\nu x}\xi} d\xi \end{array} \right] \\ T &= t - \beta_{1\mu x} L; \quad \nu = 3 - \mu\ ; \quad \nu,\, \mu \in \{1,\ 2\} \end{aligned} \tag{7}$$

each directed to a photodetector in a balanced photodetector (BPD) module. The voltage due to the BPD was expressed as (see eq. (20) in ref. [9])

$$\begin{aligned} V(\tau_m) &\propto \Re\mathrm{e}\ [\mathbf{A}_2(L,\tau_m) \bullet \mathbf{A}_2^*(L,\tau_{m-1})] \\ \mathbf{A}_2(L,\tau_r) &= \mathbf{x}A_{2x}(L,\tau_r) + \mathbf{y}A_{2y}(L,\tau_r) \\ \tau_r &= T - r/R_s; \quad r \in \{m-1, m\} \end{aligned} \tag{9}$$

where R_s is the system symbol-rate. This was based solely on the field envelopes of the QTE- and QTM-modes (7), and may be true for a nearly isotropic nonlinear fiber spliced to standard (SMF-28) single-mode fiber. However, for a device such as the $Al_{0.18}Ga_{0.82}As$ waveguide, the above expression may have to incorporate the effects of the anisotropy, which would manifest in the spatial profiles of the QTE- and QTM-modes. The more accurate expression may be derived from the divergence theorem

$$\begin{aligned} V(\tau_m) \propto R\,\Re\mathrm{e} \oiint & [\rho_\Sigma(\omega) h_\Sigma \otimes \mathbf{E}_\Sigma \times \mathbf{H}_\Sigma^* \\ & - \rho_\Delta(\omega) h_\Delta \otimes \mathbf{E}_\Delta \times \mathbf{H}_\Delta^*] \bullet \mathbf{dS} \end{aligned} \tag{10}$$

where dS = z*dxdy, R* is the BPD RF resistance, h the detector impulse response, ρ the responsivity of a detector in the BPD at the probe optical frequency ω, and

$$\begin{aligned} \mathbf{U}_\Sigma &= \mathbf{U}(\mathbf{r},\tau_m) + e^{i\phi}\mathbf{U}(\mathbf{r},\tau_{m-1}) \\ \mathbf{U}_\Delta &= \mathbf{U}(\mathbf{r},\tau_m) - e^{i\phi}\mathbf{U}(\mathbf{r},\tau_{m-1}) \end{aligned} \tag{11}$$

where $\mathbf{U}$ is either $\mathbf{E}$ or $\mathbf{H}$. The integrand in (10) expresses the differential output Poynting vector of the BPD, whose inputs are, respectively, the outputs of the constructive (Σ) and destructive (Δ) ports of the AMZI. In (11), the AMZI bias is expressed by ϕ. The EM-field of the probe in the fiber is represented collectively by $\mathbf{E}$ and $\mathbf{H}$. Under the assumptions that the differences between the two detectors in the BPD are practically negligible, and the probe power is bit-invariant, substitution of (11) into the integrand of (10) yields,

$$\begin{aligned} & \mathbf{E}_\Sigma \times \mathbf{H}_\Sigma^* - \mathbf{E}_\Delta \times \mathbf{H}_\Delta^* \\ & = 2\sum_{n=0}^{1} \mathbf{E}(\mathbf{r},\tau_{m+n-1}) \times \mathbf{H}^*(\mathbf{r},\tau_{m-n}) e^{i(1-2n)\phi} \end{aligned} \tag{12}$$

so finally,

$$\begin{aligned} & V(\tau_m) \propto \\ & R \cdot \rho(\omega) \cdot h(\tau_m) \otimes \Re\mathrm{e} \sum_{n=0}^{1} \oiint \mathbf{E}(\mathbf{r},\tau_{m+n-1}) \\ & \quad \times \mathbf{H}^*(\mathbf{r},\tau_{m-n}) e^{i(1-2n)\phi} \bullet \mathbf{dS} \end{aligned} \tag{13}$$

The semiconductor waveguide [9] presents several difficulties. The waveguide is geometrically anisotropic, although the material itself is considered isotropic. The material is also practically loss-less, because the bandgap energy of the core layer was designed to be larger than twice the photon energy of the signal. The residual losses $\alpha_{\mu\sigma}$ in (7) are mostly ascribed to waveguide side-wall roughness that results in scattering over the course of propagation. For the waveguide, the phase-index birefringence B is $\approx 10^{-2}$, much larger than that for a birefringent nonlinear fiber ($\approx 10^{-5}$) such as the photonic crystal fiber (PCF) [13]. Coupling to standard fiber from the waveguide is also indirect, across a free-space gap. The coupling problem most accurately should also consider the reflection and radiation modes at the waveguide-air junction [14], [15]. At the waveguide output facet, the QTE and QTM modes experience diffraction over the gap between the waveguide and the output fiber [16]. In this case, vector-diffraction theory should be used [17]–[19], due to the polarized nature of the light emitted by the waveguide. Further, the length scales of the device geometries, and the close proximity of the waveguide relative to the output fiber are all of the order of the wavelength $\lambda \approx 1.55\ \mu$m. In particular, the waveguide cross-section is only $1.2\ \mu\mathrm{m} \times 1.7\ \mu\mathrm{m}$, while the fiber-waveguide free-space gap is $<10\ \lambda$, which renders the simpler Fresnel (scalar) diffraction theory inaccurate [17]. For these reasons, the fields computed in (8) are instead launched by the waveguide into the gap using the Stratton–Chu vector diffraction theory [19], [20]. Reflections at the waveguide-air boundary can be neglected for a waveguide facet treated with an anti-reflection (AR) coating. For a homogeneous source-free region, the EM-field of a waveguide mode at an observation plane located at a distance $|\mathbf{r} - \mathbf{r}'|$ from the waveguide, for either the pump ($\omega = \omega_1$) or the probe ($\omega = \omega_2$) is given by

$$\begin{aligned} \mathbf{E}(\mathbf{r}) = & -\frac{1}{i\omega\varepsilon_0} \oint_{C'} \nabla' G(\mathbf{r},\mathbf{r}') \mathbf{H}(\mathbf{r}') \bullet dl' \\ & - \int_{S'} \begin{bmatrix} i\omega\mu_0 \left(\mathbf{n} \times \mathbf{H}(\mathbf{r}')\right) G(\mathbf{r},\mathbf{r}') \\ - \left(\mathbf{n} \times \mathbf{E}(\mathbf{r}')\right) \times \nabla' G(\mathbf{r},\mathbf{r}') \\ - \left(\mathbf{n} \bullet \mathbf{E}(\mathbf{r}')\right) \nabla' G(\mathbf{r},\mathbf{r}') \end{bmatrix} dS' \\ \mathbf{H}(\mathbf{r}) = & \frac{1}{i\omega\mu_0} \oint_{C'} \nabla' G(\mathbf{r},\mathbf{r}') \mathbf{E}(\mathbf{r}') \bullet dl' \\ & + \int_{S'} \begin{bmatrix} i\omega\varepsilon_0 \left(\mathbf{n} \times \mathbf{E}(\mathbf{r}')\right) G(\mathbf{r},\mathbf{r}') \\ + \left(\mathbf{n} \times \mathbf{H}(\mathbf{r}')\right) \times \nabla' G(\mathbf{r},\mathbf{r}') \\ + \left(\mathbf{n} \bullet \mathbf{H}(\mathbf{r}')\right) \nabla' G(\mathbf{r},\mathbf{r}') \end{bmatrix} dS' \end{aligned} \tag{14}$$

where $\mathbf{n}$ is the unit-normal to the surface S enclosing the point $\mathbf{r}$ in the observation plane. The aforementioned integral expression may be considered as a transformation from the r'-plane (the output plane of the waveguide) to the $\mathbf{r}$-plane (the input plane of the fiber), which is where the closed surface S' terminates. Equation (14) will be referred to as the Stratton–Chu transform (SCT). The EM-field ($\mathbf{E}$, $\mathbf{H}$)($\mathbf{r}'$) is that at the output plane of the waveguide, given by (8). The area integral is carried out over the effective exit aperture of the waveguide, while the line integral is carried out over the boundary of that aperture. The line-integrals are employed to resolve the singularity of the free-space Green's function G,

$$G(\mathbf{r},\mathbf{r}') = \frac{\exp\left(ik\,|\mathbf{r} - \mathbf{r}'|\right)}{4\pi\,|\mathbf{r} - \mathbf{r}'|} \tag{15}$$

where k is the wave number. Both the Green's function and its gradient are discontinuous at $\mathbf{r} = \mathbf{r}'$, which is the physical location of the source [21]. Moreover, since the coupling geometry is dimensionally similar to the wavelength, the contribution due to

the line-integrals may not be negligible [21]. According to Tai, however [22], Meixner's edge condition [23] renders the line integrals in (14) inconsequential for most physically realizable geometries.

The EM-field impinging on the detector is the field (**E, H**) propagating in the fiber, which may be expressed in terms of the diffracted field (14) incident at the input coupling plane of the fiber. To arrive at an analytical result that demonstrates the dependence of the detected voltage on the spatial profiles of the modes, evaluation of the SCT (14) would be required. However, an approximate approach to the solution may be found that considers the waveguide to be butt-coupled to the fiber, which also allows the solution to be adaptable to a birefringent fiber spliced to a standard fiber, such as the PCF [13]. This approximation affects the coupling coefficients, which will differ from those for the case accounting for free-space diffraction through the SCT (14). The EM-field of a σ-polarization mode in the waveguide is expressed as ($\mathbf{E}_\sigma$, H_σ), and is given and explained by (8). Unlike a highly birefringent waveguide whose principle axes are fixed along its length, the standard fiber is considered to consist of numerous sections of birefringent fibers (each with its own principle axes) oriented randomly relative to each other [3]. The fiber EM-field (**E, H**) is fully known *a priori*, and consists of a superposition of the well-known HE_{11x} and HE_{11y} modes [16]. At the waveguide-fiber junction at $z = L$, the following boundary conditions apply

$$\begin{aligned}
&\mathbf{z}\times\left[\begin{array}{c}\displaystyle\sum_{\sigma=x}^{y}\left(c_\sigma+\Gamma_\sigma e^{2i\beta_\sigma L}\right)\mathbf{E}_\sigma(\mathbf{r})\\ +\displaystyle\iint\left(c(\boldsymbol{\rho})+\Gamma(\boldsymbol{\rho})e^{2i\beta_n(\boldsymbol{\rho})L}\right)\mathbf{E}(\boldsymbol{\rho},\boldsymbol{r})\,(d\rho)^2\end{array}\right]\\
&\quad=\mathbf{z}\times\left[\sum_{\sigma=x}^{y}\mathrm{T}_\sigma\mathbf{E}_{f\sigma}(\mathbf{r})+\iint\mathrm{T}(\boldsymbol{\rho})\mathbf{E}_f(\boldsymbol{\rho},\mathbf{r})\,(d\rho)^2\right];\\
&\left[\begin{array}{c}\displaystyle\sum_{\sigma=x}^{y}\left(c_\sigma-\Gamma_\sigma e^{2i\beta_\sigma L}\right)\mathbf{H}_\sigma(\mathbf{r})\\ +\displaystyle\iint\left(c(\boldsymbol{\rho})-\Gamma(\boldsymbol{\rho})e^{2i\beta_n(\boldsymbol{\rho})L}\right)\mathbf{H}(\boldsymbol{\rho},\mathbf{r})\,(d\rho)^2\end{array}\right]\times\mathbf{z}\\
&\quad=\left[\sum_{\sigma=x}^{y}\mathrm{T}_\sigma\mathbf{H}_{f\sigma}(\mathbf{r})+\iint\mathrm{T}(\boldsymbol{\rho})\mathbf{H}_f(\boldsymbol{\rho},\mathbf{r})\,(d\boldsymbol{\rho})^2\right]\times\mathbf{z}\\
&(\boldsymbol{\rho})=(\rho_x,\rho_y);\quad(d\rho)^2=d\rho_x d\rho_y\,\cdot
\end{aligned}\tag{16}$$

The aforementioned equation includes reflection and radiation modes [14], [15], [24], [25]. In the LHS of (16), The EM-field ($\mathbf{E}_\sigma$, $\mathbf{H}_\sigma$) in the waveguide is explicitly expressed as an expansion of the QTE($\sigma = x$)- and QTM($\sigma = y$)-modes, with coefficients given by c_σ. The QTE and QTM guided modes are accompanied by radiation modes, which are represented by a double-integration over the continuous variables ρ_x and ρ_y. A portion of the EM-field ($\mathbf{E}_\sigma$, $\mathbf{H}_\sigma$) is reflected at the junction, and is expressed by the reflection coefficient Γ_σ for the discrete modes, and by $\Gamma(\boldsymbol{\rho})$ for the radiation modes. For the RHS of (16), the power coupled from the waveguide to the fiber excites the EM-field (**E, H**) through the transmission coefficient T_σ, which consists of the guided $\mathrm{HE}_{11\sigma}$-modes ($\sigma = x, y$), along with the radiation modes through the transmission coefficient $\mathrm{T}(\boldsymbol{\rho})$. The EM-field of the guided modes in the fiber is described by ($\mathbf{E}_{f\sigma}$, $\mathbf{H}_{f\sigma}$), such that ($\mathbf{E}_{fx}$, $\mathbf{H}_{fx}$) refers to the EM-field of the HE_{11x}-mode, while ($\mathbf{E}_{fy}$, $\mathbf{H}_{fy}$) refers to the EM-field of the HE_{11y}-mode. Due to the circular symmetry of the fiber, its EM-field would be expressed in cylindrical coordinates, but this is not explicitly shown in the RHS of (16). To arrive at an analytical result, several simplifying assumption can be made. It will be assumed that most of the power is carried by guided modes in both the waveguide and the fiber. Reflection modes will be considered to be relatively negligible, since the waveguide facet is considered to be treated with an AR-coating to optimize transmission to the fiber, which is a realistic assumption. The output fiber facet is considered likewise. It will also be assumed that the HE_{11x} and the HE_{11y} modes are excited equally on average so that $\mathrm{T}_x = \mathrm{T}_y = \mathrm{T}$. Under these assumptions, equation (16) simplifies to

$$\begin{cases}\mathbf{z}\times(C_x\mathbf{E}_x+C_y\mathbf{E}_y)=\mathbf{z}\times\mathbf{E}\\ (C_x\mathbf{H}_x+C_y\mathbf{H}_y)\times\mathbf{z}=\mathbf{H}\times\mathbf{z}\end{cases}\tag{17}$$

where the EM-field of the fiber is given by the two $\mathrm{HE}_{11\sigma}$ modes

$$\mathbf{U}=\sum_{\sigma=x}^{y}\mathbf{U}_{f\sigma}(\mathbf{r});\mathbf{U}\in\{\mathbf{E},\mathbf{H}\}.\tag{18}$$

The field dependence on ($\mathbf{r}$, ω, τ_m) has been suppressed for compactness. The new coupling coefficient C_σ is expressed in terms of the original coupling coefficient c_σ in (16), as c_σ/T. To resolve the coupling coefficients C_σ, the orthogonality relation for modes is invoked. For a junction between two dissimilar, but loss-less waveguides r and s, and for non-degenerate, $+z$-propagating modes σ and η [24]–[28],

$$\begin{aligned}
\left\langle\mathbf{E}_{r\sigma},\mathbf{H}^*_{s\eta}\right\rangle+\left\langle\mathbf{E}^*_{s\eta},\mathbf{H}_{r\sigma}\right\rangle&=4P_\sigma\cdot\delta_{sr}\delta_{\eta\sigma}\\
&+\omega\frac{1-\delta_{sr}}{\beta_{r\sigma}-\beta_{s\eta}}\iint(\varepsilon_r-\varepsilon_s)\,\mathbf{E}^*_{s\eta}\bullet\mathbf{E}_{r\sigma}\\
&+(\mu_r-\mu_s)\,\mathbf{H}^*_{s\eta}\bullet\mathbf{H}_{r\sigma}dS\\
\sigma,\eta&\in\{x,y\}
\end{aligned}\tag{19}$$

which represents a measurable, physical power P_σ (Watts), in the same waveguide ($s = r$), and for the same mode ($\eta = \sigma$). For dissimilar modes ($\eta \neq \sigma$) in the same waveguide ($s = r$), the equation resolves to zero. For modes in different waveguides ($s \neq r$), only the second term on the RHS of (19) survives. In general, ε the permittivity and μ the permeability (both of which are considered isotropic) are functions of the transverse coordinates and may not be factored outside the surface integral. Equation (19) represents a power-orthogonality relation. Another orthogonality relation for modes which will be useful later is obtainable by considering one of the modes in (19) to be backward-propagating, which reverses the signs of its longitudinal electric field component, its transverse magnetic field component, and that of its propagation constant. The resultant equation is similar in form to (19), and when subtracted from

(19) yields [24], [25]

$$\left\langle \mathbf{E}_{r\sigma}, \mathbf{H}^*_{s\eta} \right\rangle = S_\sigma \cdot \delta_{sr}\delta_{\eta\sigma} + \omega \frac{\delta_{sr}-1}{\beta^2_{r\sigma}-\beta^2_{s\eta}} \iint \times \begin{pmatrix} (\varepsilon_r - \varepsilon_s)\left(\beta_{r\sigma}\mathbf{E}^*_{s\eta t} \bullet \mathbf{E}_{r\sigma t} + \beta_{s\eta}\mathbf{E}^*_{s\eta z} \bullet \mathbf{E}_{r\sigma z}\right) \\ +(\mu_r - \mu_s)\left(\beta_{s\eta}\mathbf{H}^*_{s\eta t} \bullet \mathbf{H}_{r\sigma t} + \beta_{r\sigma}\mathbf{H}^*_{s\eta z} \bullet \mathbf{H}_{r\sigma z}\right) \end{pmatrix} dS \tag{20}$$

where S_σ is the complex power, while physically measurable power P_σ is obtainable by taking the real-part of (20). The subscript t denotes a transverse component, while the subscript z, a longitudinal component. In both (19) and (20), the Kronecker-δ factor is always evaluated before its coefficient to determine the applicability of each of the two RHS terms. When the absorption loss is non-negligible (as for Si nanowires/waveguides [29], [30]), similar orthogonality relations apply that involve no complex-conjugated quantities unlike (19) and (20) [24], [25]. In that case, the relations no longer represent physically measurable powers like (19) and (20). For both orthogonality relations (19), (20) and later parts of this report, the inner product is used,

$$\left\langle \mathbf{U}_\sigma, \mathbf{V}^*_\eta \right\rangle = \iint \mathbf{U}_\sigma \times \mathbf{V}^*_\eta \bullet \mathbf{dS}; \quad \mathbf{dS} = \mathbf{z}dxdy\cdot \tag{21}$$

Although not explicitly stated, since the differential area is in the transverse plane, it should be clear that only the transverse components of the EM-field may participate in a cross-product, otherwise the inner product vanishes. By contrast, all six components of the EM-field (8) are generally required for the second terms on the RHS of (19) and (20). Based on (8), (20), and (21), the complex instantaneous power S_σ can be expressed as

$$S_\sigma = |A_\sigma(L,\tau_m)|^2 \, I_\sigma \tag{22}$$

where the spatial integral

$$I_\sigma = \iint M_{\sigma x}(\mathbf{r},\omega)N^*_{\sigma y}(\mathbf{r},\omega) - M_{\sigma y}(\mathbf{r},\omega)N^*_{\sigma x}(\mathbf{r},\omega)dS \quad \sigma \in \{x,\, y\}\cdot \tag{23}$$

Now taking the post-cross-product with $\mathbf{H}^*_y$ of the electric field of (17) $\mathbf{E}$ in the fiber, and the pre-cross-product with $\mathbf{E}^*_y$ of the magnetic field of (17) $\mathbf{H}$, adding the resultant equations and integrating over the entire *xy*-coordinate (transverse) space

$$C_x\left(\left\langle \mathbf{E}_x, \mathbf{H}^*_y \right\rangle + \left\langle \mathbf{E}^*_y, \mathbf{H}_x \right\rangle\right) + C_y\left(\left\langle \mathbf{E}_y, \mathbf{H}^*_y \right\rangle + \left\langle \mathbf{E}^*_y, \mathbf{H}_y \right\rangle\right) = \left\langle \mathbf{E}, \mathbf{H}^*_y \right\rangle + \left\langle \mathbf{E}^*_y, \mathbf{H} \right\rangle \cdot \tag{24}$$

Due to the orthogonality relation (19), the first term on the RHS vanishes, since its inner products involve fields of different polarization modes in the same waveguide. Consequently, the coupling coefficient for the QTM-mode is given by

$$C_y = \frac{\left\langle \mathbf{E}, \mathbf{H}^*_y \right\rangle + \left\langle \mathbf{E}^*_y, \mathbf{H} \right\rangle}{4P_y}. \tag{25}$$

In the numerator of (25), each inner product actually consists of two inner products, due to the fact that the EM-field (**E, H**) of the fiber is described by a superposition of the HE_{11x} and HE_{11y} modes. The numerator is given by only the second term in the RHS of (19). The coupling coefficient for the QTE-mode is found from the post-cross-product with $\mathbf{H}^*_x$ of the electric field (17) $\mathbf{E}$ in the fiber, and from the pre-cross-product with $\mathbf{E}^*_x$ of the magnetic field (17) $\mathbf{H}$ in the fiber, and adding and integrating over the entire *xy*-coordinate space as for the QTM-mode. However, the solution is also obtainable from C_y simply by interchanging y and x, and the waveguide QTM-field with the waveguide QTE-field:

$$C_x = \frac{\langle \mathbf{E}, \mathbf{H}^*_x \rangle + \langle \mathbf{E}^*_x, \mathbf{H} \rangle}{4P_x}. \tag{26}$$

It is observed that coupling coefficient (25), (26) C_σ is determined by the entire EM-field (**E, H**) in the output fiber, as well as the entire EM-field ($\mathbf{E}_\sigma$, $\mathbf{H}_\sigma$) (8) for a σ-polarization mode output by the waveguide. Equations (25) and (26) are also obtainable using only (20), but the coupling coefficients would have then required some algebraic simplification to reduce them to (25) and (26).

After substituting the EM-field (**E, H**) of the fiber into (13) for the DBPSK voltage, with the AMZI bias set to π,

$$V(\tau_m) \propto R\cdot\rho(\omega)\cdot h(\tau_m) \otimes \Re\mathrm{e}\sum_{n=0}^{1}\langle \mathbf{E}(\mathbf{r},\tau_{m+n-1}), \mathbf{H}^*(\mathbf{r},\tau_{m-n})\rangle. \tag{27}$$

Since the EM-field of the fiber is expressible in terms of the $\mathrm{Al}_{0.18}\mathrm{Ga}_{0.82}\mathrm{As}$ waveguide modes according to (17), the DBPSK voltage may be re-expressed explicitly in terms of those modes:

$$V(\tau_m) \propto R\cdot\rho(\omega)\cdot h(\tau_m) \otimes \sum_{n=0}^{1}\Re\mathrm{e}\begin{bmatrix} |C_x|^2\langle \mathbf{E}_x(\mathbf{r},\tau_{m+n-1}), \mathbf{H}^*_x(\mathbf{r},\tau_{m-n})\rangle \\ +|C_y|^2\langle \mathbf{E}_y(\mathbf{r},\tau_{m+n-1}), \mathbf{H}^*_y(\mathbf{r},\tau_{m-n})\rangle \\ +C_xC^*_y\langle \mathbf{E}_x(\mathbf{r},\tau_{m+n-1}), \mathbf{H}^*_y(\mathbf{r},\tau_{m-n})\rangle \\ +C^*_xC_y\langle \mathbf{E}_y(\mathbf{r},\tau_{m+n-1}), \mathbf{H}^*_x(\mathbf{r},\tau_{m-n})\rangle \end{bmatrix}. \tag{28}$$

Now the orthogonality relation (20) instead of (19) is invoked to eliminate the third and fourth terms, since the fields are separable in time and space according to (8),

$$V(\tau_m) \propto R\cdot\rho(\omega)\cdot h(\tau_m) \otimes \sum_{n=0}^{1}\Re\mathrm{e}\begin{bmatrix} |C_x|^2\langle \mathbf{E}_x(\mathbf{r},\tau_{m+n-1}), \mathbf{H}^*_x(\mathbf{r},\tau_{m-n})\rangle \\ +|C_y|^2\langle \mathbf{E}_y(\mathbf{r},\tau_{m+n-1}), \mathbf{H}^*_y(\mathbf{r},\tau_{m-n})\rangle \end{bmatrix} \tag{29}$$

The remaining inner products are each recognized as pulse-power (19) upon the application of the real-operator. When the material absorption is non-negligible, the cross-terms in (28) survive in general, due to the fact that different orthogonality

relations from (19) and (20) apply [24], [25], [28]. After substituting the expressions for the fields from (8),

$$V(\tau_m) \propto I_x \left|C_x\right|^2 \cdot h(\tau_m) \otimes p_{xx}(\tau_m) \cos\left(\Delta\varphi_{xx}(\tau_m)\right) + I_y \left|C_y\right|^2 \cdot h(\tau_m) \otimes p_{yy}(\tau_m) \cos\left(\Delta\varphi_{yy}(\tau_m)\right) \tag{30}$$

where I_x and I_y are given in (23), and

$$\begin{aligned} p_{\sigma\sigma}(\tau_m) &= R \cdot \rho(\omega) \cdot \left|A_\sigma(L, \tau_{m-1}) A_\sigma^*(L, \tau_m)\right| \\ \Delta\varphi_{\sigma\sigma}(\tau_m) &= \varphi_\sigma(\tau_{m-1}) - \varphi_\sigma(\tau_m) \\ \sigma &\in \{x, y\} \end{aligned} \tag{31}$$

and the units of the received pulse $p_{\sigma\sigma}$ is Volts. The probe phase φ are found from the exp-factors in the solution of the NLSE (7). For a weakly birefringent device such as the PCF ($B \approx 10^{-5}$) [13], it is arguable that the coupling coefficients (25), (26) are nearly identical due to the similarities of the eigenvalues of the QTE- and QTM-modes,

$$C_x \approx C_y \tag{32}$$

while a similar argument would also hold for the spatial integrals I_x and I_y (23). This approximation reduces the DBPSK voltage (30), to (22) in [9], within a convolution with the detector impulse response h:

$$V(\tau_m) \propto h(\tau_m) \otimes \begin{pmatrix} \left|A_x(L, \tau_{m-1}) A_x^*(L, \tau_m)\right| \cos\left(\Delta\varphi_{xx}(\tau_m)\right) \\ + \left|A_y(L, \tau_{m-1}) A_y^*(L, \tau_m)\right| \cos\left(\Delta\varphi_{yy}(\tau_m)\right) \end{pmatrix} \tag{33}$$

but this simplification may be unjustifiable for a highly birefringent, anisotropic waveguide such as the $Al_{0.18}Ga_{0.82}As$ waveguide considered in [9] or a Si nanowire [29], [30], when B is a factor of $\approx 10^3$–10^4 larger than that of the PCF, and it may be more accurate to use (30) instead. The anisotropy of the coupling coefficients for the $Al_{0.18}Ga_{0.82}As$ waveguide is investigated in the following discussion.

In the waveguide, the phase of a probe pulse acquires the power profile of the RZ-OOK pump during the occurrence of a ONE, in accord with (7). The FWHM of the pump was estimated to be larger than the FWHM of the probe by a factor of >5, so the XPM-induced phase was practically flat over the duration of a probe pulse. The FWHM of the probe pulse was incorrectly stated as 2 ps in [9, Table II], while the actual FWHM was 2.3 ps. As previously noted [9], in a standard receiver before the clock/data recovery module, the FWHM pulse-width of the probe is broadened to the impulse response FWHM of the receiver opto-electronics which can be greater than $1/3R_s$ GHz^{-1} (Baud-rate R_s in GB), and more than a factor of 10 larger than the DGD (0.9 ps) of the waveguide in the C-band [9]. Consequently, DGD effects can be considered negligible. The walk-off length was also found to be much larger than the physical length using the FV-FDM [4], and its effect is thus also negligible. Moreover, the SPM-induced phase shifts in (7) are bit-independent, regardless of probe polarization. Consequently, the differential phase reduces to that for XPM, after differential detection. These simplifying assumptions reduce the integrals to effective lengths in (7), the solution of the NLSE.

At the m-th sampling instant, the corrected detected DBPSK voltage acquires the following form (see Eq. (24) in [9]), after a normalization by the bit-invariant pulse power,

$$\begin{aligned} &V(\tau_m, \theta_1) \propto \\ &10^{-PDL/10} \cdot J \cdot \cos^2\theta_2 \cos\left(\left(2\gamma_{21xx} P_{01} L_{\mathrm{eff}\,x}\right) \Delta\psi_x \right. \\ &\quad \left. + \left(\gamma_{21xy} P_{01} L_{\mathrm{eff}\,y}\right) \Delta\psi_y\right) \\ &\quad + \sin^2\theta_2 \cos\left(\left(\gamma_{21yx} P_{01} L_{\mathrm{eff}\,x}\right) \Delta\psi_x + \left(2\gamma_{21yy} P_{01} L_{\mathrm{eff}\,y}\right) \Delta\psi_y\right) \end{aligned} \tag{34}$$

where

$$J = \frac{I_x \cdot \left|C_x\right|^2}{I_y \cdot \left|C_y\right|^2} \tag{35}$$

is the coupling coefficient ratio, and

$$\begin{aligned} \Delta\psi_\sigma &= a_m \cdot \cos^2\left(\theta_1(\tau_m) - \frac{\pi}{2}\delta_{\sigma y}\right) \\ &\quad - a_{m-1} \cdot \cos^2\left(\theta_1(\tau_{m-1}) - \frac{\pi}{2}\delta_{\sigma y}\right) \\ \sigma &\in \{x, y\}; \quad a_m \in \{0, 1\} \forall\, m. \end{aligned} \tag{36}$$

The nonlinear coefficients are found from Table I. The correction in (34) relative to (24) in the original paper [9] includes contributions due to the coupling coefficients (25), (26), and the overlap integrals I_x and I_y given by (23). These integrals for the $Al_{0.18}Ga_{0.82}As$ waveguide have been computed using FV-FDM [4], and were found to differ by $\approx 3.5\%$.

The following analysis assumes that the pump peak power is sufficient to generate a π phase-shift for a RZ-OOK pump launched along the lower loss y-axis of the waveguide. For the $Al_{0.18}Ga_{0.82}As$ waveguide, this axis is the [0 0 1] crystallographic direction, which corresponds to the QTM-mode. Thus

$$\left[(a_n - a_{n-1}) \cdot 2\gamma_{1yy} P_{01} L_{\mathrm{eff}y}\right] = \pi. \tag{37}$$

This also assumes a ONE-ZERO or a ZERO-ONE transition (which is the most frequent pattern [31]) in the RZ-OOK pump. The polarization dependent loss (*PDL*) was measured to be 0.75 dB [9]. To estimate the launch angle θ_2 of the probe that corresponds to the minimum voltage fluctuation in (34) or equivalently, polarization-insensitive XPM in the waveguide, the launch angle θ_1 of the pump (which was polarization-scrambled in the experiment [9]) is swept over 0°–90° while the ratio J (35) is held fixed. The result is summarized in Fig. 3, which shows that for the experimentally measured probe launch angle of 40°, the ratio J is approximately 1.1. After disregarding in (35) the (I_x/I_y) ratio that was estimated to be ≈1.035 based on FV-FDM [4], J is reduced to 1.063, which is still practically ≈1.1. The behavior of the detected voltage for $J = 1.1$ is shown in Fig. 4, and demonstrates that the minimum fluctuation is indeed attained at ≈40°. In [9], the waveguide PDL was measured using the Fabry–Perot method [32] prior to the application of the AR coating, and found to be ≈0.75 dB. The method is considered to be independent of coupling efficiency,

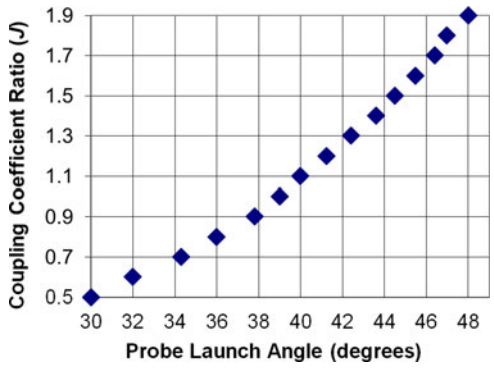

Fig. 3. Coupling coefficient ratio (J) versus the probe launch angle (θ_2), as the pump launch angle (θ_1) is swept over 0°–90°.

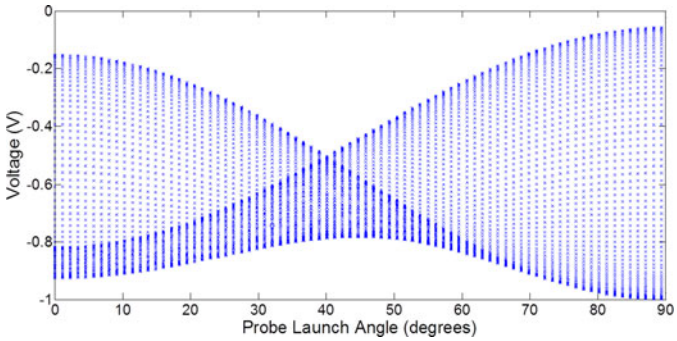

Fig. 4. Detector voltage [equation (34)] versus probe launch angle (θ_2), while the pump launch angle (θ_1) is varied over 0°–90°, and the coupling coefficient ratio J is fixed at 1.1. The minimum fluctuation is seen to occur at $\theta_2 \approx 40°$.

for a waveguide with well-cleaved facets. Subsequently, coupling to the AR-coated waveguide was achieved using lensed fibers, which had negligible PDL (0.1 dB maximum). In that experiment, it was possible to adjust the state of polarization of the light coupled to the waveguide using a mechanical polarization controller, which yielded a maximum power variation of ≈0.75 dB at the output lensed fiber. This experiment suggested that the coupling efficiencies of the QTE- and QTM-modes to the fiber were quite similar within experimental error, and this observation also accounts for diffraction [according to (14)] over the air-gap between the waveguide facets and the lensed fibers. The small discrepancy (≈3%) between the theoretical coupling coefficients C_x and C_y is then attributed to diffraction, and residual junction reflection and radiation modes, all of which are neglected in the theoretical treatment.

III. Conclusion

In our original paper [9], besides the errors in the nonlinear coefficients in Section III, eq. (22) for the detected DBPSK voltage was found to be accurate only for a birefringent fiber such as the PCF [13]; but may be different in general for the case of a relatively higher-birefringence waveguide such as another AlGaAs waveguide [33], or a Si nanowire [29], [30]. These errors affect all equations beyond (22) in [9]. In the absence of diffraction, theory indicates that the measured probe launch angle of ≈40° that was required for polarization-insensitive XPM occurs for a waveguide-fiber coupling efficiency ratio $|C_x / C_y|^2$ of ≈1.1, for the QTE-mode relative to the QTM-mode. This demonstrated good agreement with the experimentally observed ratio of ≈1, and validated the theoretical approach. Therefore for the AlGaAs waveguide of [9], its design ultimately ensured that the power coupled to the output lensed fiber was independent of polarization.

References

[1] S. Kumar, A. Selvarajan, and G. Anand, "Nonlinear propagation of two optical pulses of two different frequencies in birefringent fibers," *J. Opt. Soc. Amer. B*, vol. 11, pp. 810–817, 1994.

[2] G. P. Agrawal, *Nonlinear Fiber Optics*, 3rd ed. San Diego, CA, USA: Academic Press, ch. 7 and 10, 2001.

[3] K. Inoue, "Polarization effect on four-wave mixing efficiency in a single-mode fiber," *IEEE J. Quantum Electron.*, vol. 28, no. 4, pp. 883–895, Apr. 1992.

[4] A. B. Fallahkhair, K. S. Li, and T. E. Murphy, "Vector finite difference modesolver for anisotropic dielectric waveguides," *J. Lightw. Technol.*, vol. 26, no. 11, pp. 1423–1431, Jun. 2008.

[5] D. C. Hutchings, A. S. Aitchison, B. S. Wherrett, G. T. Kennedy, and W. Sibbett, "Polarization dependence of ultrafast nonlinear refraction in an AlGaAs waveguide at the half-band gap," *Opt. Lett.*, vol. 20, pp. 991–993, 1995.

[6] J. S. Aitchison, D. C. Hutchings, J. U. Kang, G. I. Stegeman, and A. Villeneuve, "The nonlinear optical properties of AlGaAs at the half band gap," *IEEE J. Quantum Electron.*, vol. 33, no. 3, pp. 341–349, Mar. 1997.

[7] J. U. Kang, G. I. Stegeman, A. Villeneuve, and J. S. Aitchison, "AlGaAs below half bandgap: A laboratory for spatial soliton physics," *Pure Appl. Opt., J. Eur. Opt. Soc. A*, vol. 5, pp. 583–594, 1996.

[8] S. Gehrsitz, F. K. Reinhart, C. Gourgon, N. Herres, A. Vonlanthen, and H. Sigg, "The refractive index of $Al_xGa_{1-x}As$ below the band gap: Accurate determination and empirical modeling," *J. Appl. Phys.*, vol. 87, p. 7825, 2000.

[9] B. M. Cannon, W. Astar, T. Mahmood, P. Apiratikul, G. A. Porkolab, C. J. K. Richardson, and G. M. Carter, "Data transfer from RZ-OOK to RZ-BPSK by polarization-insensitive XPM in a passive birefringent nonlinear AlGaAs waveguide," *J. Lightw. Technol.*, vol. 31, no. 6, pp. 952–966, Mar. 2013.

[10] R. H. Stolen and J. E. Bjorkholm, "Parametric amplification and frequency conversion in optical fiber," *IEEE J. Quantum Electron.*, vol. 18, no. 7, pp. 1062–1073, Jul. 1982.

[11] K. O. Hill, D. C. Johnson, B. S. Kawasaki, and R. I. McDonald, "CW three-wave mixing in single-mode optical fibers," *J. Appl. Phys.*, vol. 49, pp. 5098–5108, 1978.

[12] K. M. Lo and E. H. Li, "Solution of the quasi-vector wave equation for optical waveguides in a mapped infinite domains by the Galerkin's method," *J. Lightw. Technol.*, vol. 16, no. 5, pp. 937–945, May 1998.

[13] W. Astar, C.-C. Wei, Y.-J. Chen, J. Chen, and G. M. Carter, "Polarization-insensitive 40 Gb/s wavelength and RZ-OOK-to-RZ-BPSK modulation format conversion by XPM in a highly nonlinear PCF," *Opt. Exp.*, vol. 16, pp. 12039–12049, 2008.

[14] K. Matsumura and Y. Tomabechi, "Reflection and transmission characteristics of an uncoincidental junction on rectangular dielectric waveguides," *IEEE Trans. Microw. Theory Techn.*, vol. 37, no. 2, pp. 414–420, Feb. 1989.

[15] Y. Tomabechi and K Matsumura, "Reflection and transmission coefficients of rectangular dielectric waveguide discontinuity with an air gap," *IEEE Trans. Microw. Theory Techn.*, vol. 38, no. 6, pp. 797–799, Jun. 1990.

[16] K. Okamoto, *Fundamentals of Optical Waveguides*, 2nd ed. Amsterdam, Netherlands: Academic Press, ch. 2, 2005.

[17] J. W. Goodman, *Introduction to Fourier Optics*. San Fransico, CA, USA: McGraw-Hill Inc, ch. 3, 1968.

[18] F. Kottler, "Electromagnetische theorie der beugung an schwarzen schirmen," *Annalen der Physik*, vol. 47, pp. 457–508, 1923.

[19] J. A. Stratton and L. J. Chu, "Diffraction theory of electromagnetic waves," *Phys. Rev.*, vol. 56, pp. 99–108, 1932.

[20] M. Blank, K. Kreischer, and R. J. Temkin, "Theoretical and experimental investigation of a quasi-optical mode converter for a 110-GHz gyrotron," *IEEE Trans. Plasma Sci.*, vol. 24, no. 3, pp. 1058–1067, Jun. 1996.

[21] W. Hsu and R. Barakat, "Stratton-Chu vectorial diffraction of electromagnetic fields by apertures with application to small-Fresnel-number systems," *J. Opt. Soc. Amer. A*, vol. 11, pp. 623–630, 1994.
[22] C. T. Tai, "Direct integration of field equations," *Progr. Electromag. Res.*, vol. 28, pp. 339–359, 2000.
[23] J. Meixner, "Die kantenbedingung in der theorie der beugung elecktromagnetischer wellen und volkommen leitenden ebenem schirmen," *Ann. Phys.*, vol. 441, pp. 2–9, 1949.
[24] D. Marcuse, *Theory of Dielectric Optical Waveguides*. Amsterdam, Netherlands: Academic Press, ch. 1, 1974.
[25] S. F. Mahmoud, *Electromagnetic Waveguides: Theory and Applications*. London, U.K.: Peter Peregrinus Ltd., ch. 2, 3, 4, 1991.
[26] N. Engheta and P. Pelet, "Mode orthogonality in chiral waveguides," *IEEE Trans. Microw. Theory Techn.*, vol. 38, no. 11, pp. 1631–1636, Nov. 1990.
[27] A. F. Milton and W. K. Burns, "Mode coupling in optical waveguide horns," *IEEE J. Quantum Electron.*, vol. 13, no. 10, pp. 828–836, Oct. 1977.
[28] C. Dragone, "Scattering at a junction of two waveguides with different surface impedances," *IEEE Trans. Microw. Theory Techn.*, vol. 32, no. 10, pp. 1319–1325, Oct. 1984.
[29] W. Astar, J. B. Driscoll, X. Liu, J. I. Dadap, W. M. J. Green, Y. A. Vlasov, G. M. Carter, and R. M. Osgood, "All-optical format conversion of NRZ-OOK to RZ-OOK in a silicon nanowire utilizing either XPM or FWM and resulting in a receiver sensitivity gain of ≈2.5 dB," *IEEE J. Sel. Topics Quantum Electron.*, vol. 16, no. 1, pp. 234–239, Jan./Feb. 2010.
[30] M. Pu, H. Hu, C. Peucheret, H. Ji, M. Galili, L. K. Oxenløwe, P. Jeppesen, J. M. Hvam, and K. Yvind, "Polarization insensitive wavelength conversion in a dispersion-engineered silicon waveguide," *Opt. Exp.*, vol. 20, pp. 16374–16380, 2012.
[31] H. Bulow, "System outage probability due to first- and second-order PMD," *IEEE Photon. Technol. Lett.*, vol. 10, no. 5, pp. 696–699, May 1998.
[32] R. Regener and W. Sohler, "Loss in low-finesse Ti:$LiNbO_3$ optical waveguide resonators," *Appl. Phys. B*, vol. 36, pp. 143–147, 1985.
[33] K. Dolgaleva, W. C. Ng, L. Qian, and J. S. Aitchison, "Compact highly-nonlinear AlGaAs waveguides for efficient wavelength conversion," *Opt. Exp.*, vol. 19, pp. 12440–12455, 2011.

W. Astar received the B.Sc. degree in electrical engineering, the M.Sc. degree in electrical engineering, the B.Sc. degree in mechanical engineering from the University of South Florida, Tampa, FL, USA, and the Ph.D. degree in electrical engineering from the University of Maryland Baltimore County, Baltimore, MD, USA. He has held technical positions with Pall Aeropower, Inc., Antec Networks (Arris Group, Inc.) and the Ciena Corporation. He is currently with the Laboratory for Physical Sciences, and the Center for Advanced Studies in Photonics Research, both in MD, USA. His research interests include long-haul, coherent DWDM transmission, modulation formats, semiconductor devices, and ultra-fast nonlinear optical processing techniques. He has co-authored more than 30 journal publications and conference presentations, and he is a member of Tau Beta Pi, Pi Tau Sigma, and Phi Kappa Phi.

Brice M. Cannon received the B.S. degree in optical engineering and the B.S. degree in applied mathematics from Norfolk State University, Norfolk, VA, USA, as a Dozoretz National Institute for Mathematics and Sciences (DNIMAS) Scholar. He is currently working toward the Ph.D. degree in electrical engineering at the University of Maryland Baltimore County (UMBC), Baltimore, MD, USA. He is also affiliated with the Laboratory for Physical Sciences and the Center for Advanced Studies in Photonics Research. At the University of Arizona, he carried out research in the area of ultra-high density data storage optical devices fabricated from azo-dye-doped polymer films. While at the Lawrence Livermore National Laboratory and the Center for Adaptive Optics, he investigated the performance capabilities of the Large Synoptic Survey Telescope's active optics control system. He was also with The European Organization for Nuclear Research (CERN), where he worked on the design and modeling of a low energy electro-magnetic beam line for the transport of ions from the REX to the Weak-Interaction-Trap for Charged Particles experiments at ISOLDE. His current research interests include ultra-fast nonlinear optical signal processing techniques, nonlinear optics, long-haul DWDM transmission, and nonlinear birefringent devices. He is a member of Beta-Kappa-Chi, Golden Key, and NSBE.

Tanvir Mahmood recieved the B.Sc. degree in electrical and electronic engineering from the Bangladesh University of Engineering and Technology (BUET), Dhaka, Bangladesh. He is currently working toward the Ph.D. degree in electrical engineering at the University of Maryland Baltimore County (UMBC), Baltimore, MD, USA. He held technical positions with Grameenphone Ltd.; Telenor Norway based GSM Operator. He is affiliated with the Laboratory for Physical Sciences and the Center for Advanced Studies in Photonics Research. His current research interests include nonlinear optics, high-speed DWDM transmission, ultra-fast nonlinear optical signal processing and nonlinear optical devices.

Paveen Apiratikul received the B.S. degrees in electrical engineering from Chulalongkorn University, Thailand, in 1999 and the M.S. and Ph.D. degrees in electrical engineering from the University of Maryland, College Park, MD, USA, in 2002 and 2009, respectively. He is currently with Laboratory for Physical Sciences (LPS), MD. His research interests include nonlinear optical signal processing, optical semiconductor devices, numerical simulation and nanotechnology.

G. A. Porkolab biography not available at the time of publication.

C. J. K. Richardson biography not available at the time of publication.

Gary M. Carter (M'82–SM'85–F'08) received the Ph.D. degree in physics from the Massachusetts Institute of Technology (MIT), Cambridge, MA, USA, in the area of atomic and molecular beam scattering. He has carried out research in the area of infrared radar and infrared nonlinear optics at MIT's Lincoln Laboratory, Lexington. He has also investigated ultrafast processes in polymers with GTE's corporate research laboratories and coherent optical communications with MIT's Lincoln Laboratory. He was appointed to the Electrical Engineering Faculty with the University of Maryland Baltimore County (UMBC), Baltimore, MD, USA, in 1988, where he is now Chair of the Department of Computer Science and Electrical Engineering. Since 1988, he has carried out research on mode-locked lasers, biosensors, ultra-fast nonlinear optical processing, and high-speed DWDM transmission. He has authored more than 100 journal publications. He is a Life Fellow of the IEEE, a Fellow of the OSA, and is a member of the APS.